Improving Performance of All-Polymer Solar Cells Through Backbone Engineering of Both Donors and Acceptors

Improving Performance of All-Polymer Solar Cells Through Backbone Engineering of Both Donors and Acceptors

Chunhui Duan, Zhaojun Li, Shuting Pang, You-Liang Zhu, Baojun Lin, Fallon J. M. Colberts, Pieter J. Leenaers, Ergang Wang,* Zhao-Yan Sun,* Wei Ma,* Stefan C. J. Meskers, and René A. J. Janssen**

All-polymer solar cells (APSCs), composed of semiconducting donor and acceptor polymers, have attracted considerable attention due to their unique advantages compared to polymer-fullerene-based devices in terms of enhanced light absorption and morphological stability. To improve the performance of APSCs, the morphology of the active layer must be optimized. By employing a random copolymerization strategy to control the regularity of the backbone of the donor polymers (PTAZ-TPD*x*) and acceptor polymers (PNDI-T*x*) the morphology can be systematically optimized by tuning the polymer packing and crystallinity. To minimize effects of molecular weight, both donor and acceptor polymers have number-average molecular weights in narrow ranges. Experimental and coarse-grained modeling results disclose that systematic backbone engineering greatly affects the polymer crystallinity and ultimately the phase separation and morphology of the all-polymer blends. Decreasing the backbone regularity of either the donor or the acceptor polymer reduces the local crystallinity of the individual phase in blend films, affording reduced short-circuit current densities and fill factors. This two-dimensional crystallinity optimization strategy locates a PCE maximum at highest crystallinity for both donor and acceptor polymers. Overall, this study demonstrates that proper control of both donor and acceptor polymer crystallinity simultaneously is essential to optimize APSC performance.

1. Introduction

Polymer solar cells (PSCs) based on bulk-heterojunction (BHJ) concept hold the promise to be a low-cost renewable power source, possibly used in building integrated photovoltaics.[1] During the past two decades, significant progress has been achieved in improving the power conversion efficiencies (PCEs), reaching over 14% recently, via creating novel photoactive materials, optimizing active layer morphology and organic/metal interface, and device engineering.[2] Historically, the acceptor materials of PSCs were predominately limited to fullerene derivatives, which suffer from a few limitations including weak optical absorption, costly production, and poor morphological stability in BHJ films.[3] Therefore, there is a growing interest in developing and understanding non-fullerene acceptors.[4] Among these alternative acceptors, *n*-type

Prof. C. Duan, S. Pang
Institute of Polymer Optoelectronic Materials and Devices
State Key Laboratory of Luminescent Materials and Devices
South China University of Technology
510640 Guangzhou, P. R. China
E-mail: duanchunhui@scut.edu.cn

Prof. C. Duan, F. J. M. Colberts, P. J. Leenaers, Dr. S. C. J. Meskers, Prof. R. A. J. Janssen
Molecular Materials and Nanosystems, Institute for Complex Molecular Systems
Eindhoven University of Technology
P. O. Box 513, 5600 MB Eindhoven, The Netherlands
E-mail: r.a.j.janssen@tue.nl

DOI: 10.1002/solr.201800247

Dr. Z. Li, Prof. E. Wang
Department of Chemistry and Chemical Engineering
Chalmers University of Technology
SE-412 96 Göteborg, Sweden
E-mail: ergang@chalmers.se

Dr. Y.-L. Zhu, Prof. Z.-Y. Sun
State Key Laboratory of Polymer Physics and Chemistry
Changchun Institute of Applied Chemistry
Chinese Academy of Sciences
130022 Changchun, P. R. China
E-mail: zysun@ciac.ac.cn

B. Lin, Prof. W. Ma
State Key Laboratory for Mechanical Behavior of Materials
Xi'an Jiaotong University
710049 Xi'an, P. R. China
E-mail: msewma@mail.xjtu.edu.cn

Prof. R. A. J. Janssen
Dutch Institute for Fundamental Energy Research
De Zaale 20, 5612 AJ Eindhoven, The Netherlands

The ORCID identification number(s) for the author(s) of this article can be found under https://doi.org/10.1002/solr.201800247.

π-conjugated polymers were reported to have the unique advantages of tunable optoelectronic properties, controllable polymer orientation, and stable BHJ morphology.[4e,5] As a result, all-polymer solar cells (APSCs) composed of a *p*-type polymer donor and an *n*-type polymer acceptor provide opportunities for improving the device efficiency and stability simultaneously.[4e,5e,5h,6] Encouragingly, PCEs exceeding 8% for APSCs have been reported by a few groups independently.[5h,6b,7] Among the various *n*-type conjugated polymers studied as electron acceptors in APSCs, naphthalene diimide (NDI), and perylene diimide (PDI) based polymers are the most promising materials due to their high electron mobility and suitable energy levels.[7a,7c,7f] Up to date, the PCE record of APSCs is actually achieved by a NDI polymer, which is poly[[*N*,*N*′-bis(2-octyldodecyl)-naphthalene-1,4,5,8-bis(dicarboximide)-2,6-diyl]-*alt*-5,5′-(2,2′-bithiophene)] with a commercial name N2200.[7c,8]

However, the power conversion efficiencies (PCEs) of APSCs composed of NDI or PDI based polymer acceptors still lag behind that of polymer:fullerene PSCs, principally due to the difficulties in controlling the morphology of the polymer: polymer blends, which are prone to polymer-polymer demixing due to their low mixing entropy, resulting in large phase separation with a domain size much larger than the exciton diffusion length.[9] Modulating the polymer crystallization via introducing a third unit into alternating donor–acceptor (D–A) polymer main chains was reported to be a fruitful strategy to optimize the morphology of all-polymer blends.[7g,10] For example, Hwang et al.[10a] examined the effect of introducing the bulky PDI segments to replace the NDI segments in the polymer backbone to reduce the crystallinity of a NDI-selenophene polymer, which consequently led to an optimized BHJ morphology with smaller domain size and enhanced device performance. A similar replacement of NDI segments by PDI segments was also reported by Sharma et al.[10b] to reduce the crystallinity of N2200. Li et al.[10c] reported the crystallinity control of N2200 by replacing a certain amount of bithiophene units in the N2200 backbone by single thiophene units. Combined with the solvent annealing after film deposition, optimal BHJ morphology with proper phase separation was formed which further improved device performance.[10c] Although success has been achieved through molecular engineering of the polymer backbone, this strategy has been explored only for one of the two components, mainly for polymer acceptors, while keeping the second component unchanged. Notably, a rational selection of both polymer donor and acceptor simultaneously is essential to optimize and to understand the morphology of all-polymer blends.[9b,10d,11] This knowledge can further guide to the design of novel donor and acceptor polymers for high performance APSCs.

Herein, we report the backbone engineering of both donor and acceptor polymers simultaneously via introducing a third comonomer to modulate the polymer crystallinity, film morphology, photophysical properties, and device performance of the resulting APSCs. The donor polymers are derived from electron-rich benzodithiophene (BDT) and electron-deficient difluorobenzotriazole (TAZ), for which the perfectly alternating D–A polymer afforded highly efficient APSCs previously (PCEs up to 8.27%).[6f,7a] Here, we introduce a certain amount of thieno[3,4-c]pyrrole-4,6-(5H)-dione (TPD) units to replace the difluorobenzotriazole (TAZ) units as a second electron-withdrawing unit in the polymer backbone, generating a series of donor polymers PTAZ-TPD*x* (in which *x* stands for the molar percentage of TPD relative to the total amount of acceptor units) (**Scheme 1**). The reason for choosing TPD as the second acceptor unit is that the binary copolymers of BDT-TPD show similar optical absorption and energy levels as BDT-TAZ copolymers. Moreover, the binary copolymers of both BDT-TAZ and BDT-TPD afforded substantial PCEs in APSCs.[7a,7b] The acceptor polymers are based on N2200,[8] which has been extensively used in APSCs and afforded the best-performing APSCs up to date (PCEs up to 10.1%).[7a,7c,7e] We used a series of copolymers PNDI-T*x* developed in Wang's group previously, where a certain amount of bithiophene (2T) units in the N2200 backbone were replaced by single thiophene (T) as the second electron-donating units. The *x* in PNDI-T*x* represents the molar percentage of single thiophene relative to the total donor units (Scheme 1).[10c] We find that the device performance of the APSCs decreases upon reducing the regularity of the main chain of both the donor and acceptor polymers, and that the PCE is more susceptible to the regularity of the acceptor polymer. The observed trends agree well with the polymer crystallinity, phase separation morphology, and charge transport in polymer-polymer blends. The results obtained in this work provide an effective strategy for improving the device performance of APSCs. Moreover, this study

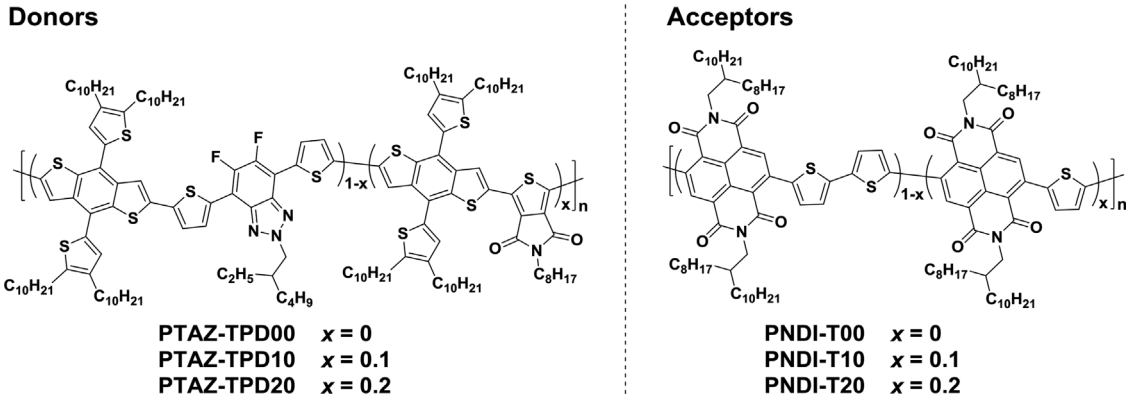

Scheme 1. Chemical structures of the donor and acceptor polymers studied in this paper. Note that PNDI-T00 is identical to N2200.

demonstrates that a proper control of the crystallinity of both donor and acceptor polymers simultaneously is essential to realize the full potential of APSCs.

2. Results and Discussion

2.1. Synthesis of PTAZ-TPD*x* and PNDI-T*x*

The donor polymers PTAZ-TPD*x* were synthesized via a Stille cross-coupling reaction using three monomers, 2,6-bis-(trimethyltin)-4,8-di(2,3-didecylthiophen-5-yl)-benzo[1,2-b:4,5-b′]dithiophene, 4,7-bis(5-bromothiophen-2-yl)-2-(2-ethylhexyl)-5,6-difluoro-2H-benzo[*d*][1,2,3]triazole, and 1,3-dibromo-5-octyl-4H-thieno[3,4-*c*]pyrrole-4,6-(5H)-dione (Figure S1, Supporting Information). The PNDI-T*x* acceptor polymers were synthesized by following our previous procedures.[10c] All polymers possess good solubility in common organic solvents, such as chloroform (CF), chlorobenzene (CB), and *ortho*-dichlorobenzene (*o*-DCB) at room temperature. The molecular weights of the polymers were measured via gel permeation chromatography (GPC) in *o*-DCB at 140 °C. As summarized in **Table 1**, the PTAZ-TPD*x* polymers have very similar number-average molecular weights of $\bar{M}_n = 29 \pm 3$ kDa and molar-mass dispersity ($Đ_M = \bar{M}_w/\bar{M}_n$) of ≈2.5, while the PNDI-T*x* polymers have $\bar{M}_n = 39 \pm 2$ kDa and $Đ_M$ of ≈2.5. It is well recognized that molecular weights of both donors and acceptors can significantly influence the device performance of APSCs.[5c,7e,9b,10c,12] The similar molecular weights and molar-mass dispersities are thus essential to enable a direct comparison and establish reliable structure–performance relationships.

2.2. Thermal, Optical, and Electrochemical Properties

The thermal properties of the PTAZ-TPD*x* and PNDI-T*x* polymers were investigated by differential scanning calorimetry (DSC). The DSC curves are depicted in Figure S3 (Supporting Information) and the thermal transition parameters are summarized in Table 1. The PTAZ-TPD*x* polymers did not show clear melting or crystallization transitions in the scanning range from 0 to 350 °C, suggesting a relatively low degree of crystallinity. In contrast, all PNDI-T*x* polymers show a clear melting transition upon heating and a corresponding crystallization transition upon cooling. The melting temperature (T_m), the crystallization temperature (T_c), and the enthalpies for melting (ΔH_m) and crystallization (ΔH_c) all drop upon increasing the *x* value in PNDI-T*x*. These results indicate that the three PNDI-T*x* polymers are semi-crystalline and that the degree of crystallinity is lowered by reducing the regularity of the polymer backbone, in line with our previous results.[10c]

The optical absorption spectra of the polymers PTAZ-TPD*x* and PNDI-T*x* are shown in **Figure 1**a and the relevant parameters are listed in Table 1. The PTAZ-TPD*x* polymers exhibit almost identical absorption spectra, but the absorption coefficients of the polymers reduce slightly upon decreasing the regularity of the polymer backbone, suggesting a slight decrease of ordering of polymer in the films. With regard to PNDI-T*x*, two distinct absorption bands at 300–450 nm and 500–850 nm are visible. These correspond to the localized electronic transitions of the aromatic backbone and the π–π* transitions with intramolecular charge transfer (ICT) character between the electron-donating and electron-withdrawing moieties, respectively. By decreasing the backbone regularity, the PNDI-T*x* polymers exhibit gradually blue-shifted absorption peaks and reduced absorption intensities. Notably, the absorption coefficients of the ICT bands of the PNDI-T*x* polymers are around $3 \times 10^4\ cm^{-1}$, which are significantly lower than that of the PTAZ-TPD*x* polymers ($\approx 6.5 \times 10^4\ cm^{-1}$).

The frontier orbital energy levels of the polymers were measured by square wave voltammetry (SWV) from the onsets of the redox waves (Figure S4, Supporting Information). The energy levels of the highest occupied molecular orbital (HOMO) and lowest unoccupied molecular orbital (LUMO) (Figure 1b and Table 1) are reported relative to the energy level of ferrocene of −5.23 eV versus vacuum.[13] We note that these values represent our estimates of the onsets of broadened HOMO and LUMO bands that span a range of energy levels. The HOMO levels of PTAZ-TPD10 and PTAZ-TPD20 are slightly more negative than PTAZ-TPD00, stemming from the slightly stronger electron-withdrawing ability of TPD unit than TAZ unit. For the PNDI-T*x* acceptor polymers, increasing *x* did not lead to any noteworthy differences in HOMO or LUMO levels, suggesting the dominant role of the electron-withdrawing NDI units. Each combination of the PTAZ-TPD*x* donor polymer and PNDI-T*x* acceptor polymer has sufficient LUMO–LUMO offsets (>0.3 eV) for efficient electron transfer from the donor to the acceptor and sufficient HOMO–HOMO offsets for efficient hole transfer from the acceptor to the donor in blends.

Table 1. Molecular weight, thermal and optical properties, and exciton lifetimes of PTAZ-TPDx and PNDI-Tx.

Polymer	M_n [kDa]	$Đ_M$	T_m [°C]	ΔH_m [J g^{-1}]	T_c [°C]	ΔH_c [J g^{-1}]	λ_{max} [nm]	λ_{onset} [nm]	E_g [eV][a)]	τ [ps]
PTAZ-TPD00	29	2.6	–	–	–	–	543, 586	640	1.94	890
PTAZ-TPD10	31	2.5	–	–	–	–	544, 586	643	1.93	730
PTAZ-TPD20	26	2.5	–	–	–	–	547, 588	644	1.93	630
PNDI-T00	41	2.8	314	7.7	287	9.1	392, 698	851	1.46	210
PNDI-T10	38	2.8	303	5.8	274	6.7	388, 684	838	1.48	260
PNDI-T20	38	2.5	282	4.3	248	5.8	386, 676	832	1.49	300

[a)] Calculated from the long-wavelength onset of the optical absorption spectra (λ_{onset}) of the polymer films via $E_g(eV) = 1240/\lambda_{onset}(nm)$. Values differ from the electrochemical bandgaps shown in **Figure 1**b.

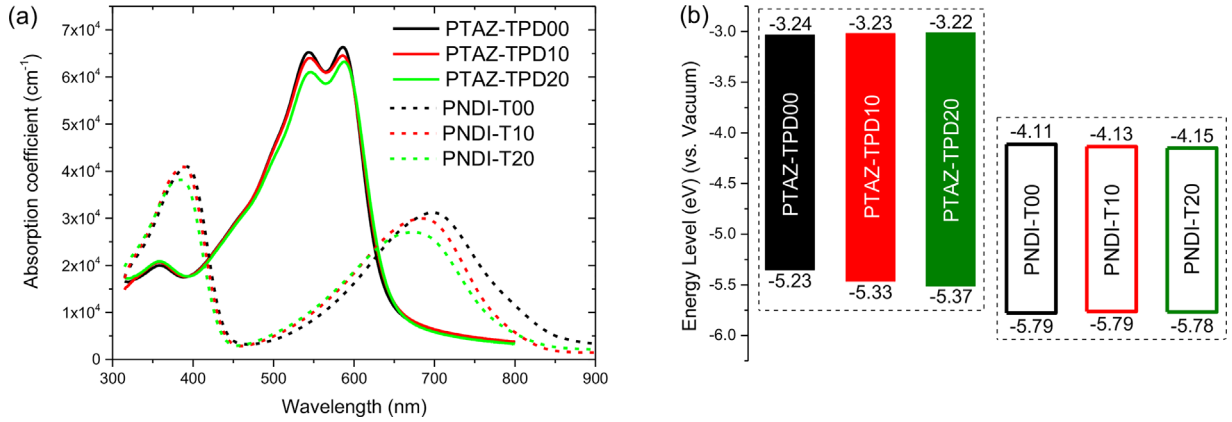

Figure 1. UV-vis-NIR absorption spectra a) and energy levels b) of the PTAZ-TPD*x* donor and the PNDI-T*x* acceptor polymers.

2.3. All-Polymer Solar Cells

The above-mentioned PTAZ-TPD*x* and PNDI-T*x* polymers were used to make all-polymer solar cells via a 3 × 3 characterization matrix. The device structure was indium tin oxide (ITO)/ZnO (30 nm)/PTAZ-TPD*x*:PNDI-T*x*/MoO_x (10 nm)/Ag (100 nm). Testing of the solar cells was performed under AM1.5G illumination (100 mW cm^{-2}). The device performance for each PTAZ-TPD*x*:PNDI-T*x* combination was fully optimized in terms of donor:acceptor weight ratio, solvent, cosolvent, and thermal annealing at different temperatures. The device metrics of the optimized APSCs are presented in **Figure 2** and **Table 2**. The current density–voltage (*J*–*V*) characteristics, and external quantum efficiency (EQE) spectra are shown in Figure S5 (Supporting Information). The device metrics acquired under various fabrication conditions are gathered in Table S3–S8 (Supporting Information).

Interestingly, we observed that a decrease of regularity of the acceptor polymers PNDI-T*x* results in a considerable drop in PCE regardless of the donor polymer used. Specifically, when using PTAZ-TPD00 as the donor polymer, the PCE of the solar cells decreased from 6.6 to 4.8% by changing the acceptor polymer from PNDI-T00 to PNDI-T20. A similar declining trend, however less pronounced, was observed when decreasing the regularity of the donor polymers, that is, increasing the *x* value in the PTAZ-TPD*x*. For example, when using PNDI-T00 as the acceptor polymer, the PCE of the solar cells decreased from 6.6% for PTAZ-TPD00 to 5.8% for PTAZ-TPD20. These trends caused by changing the regularity of the polymer backbone are exemplified by comparing PCE of the "diagonal" series (PTAZ-TPD00:PNDI-T00, PTAZ-TPD10:PNDI-T10, and PTAZ-TPD20:PNDI-T20). The open-circuit voltage (V_{oc}) of all devices are almost identical (V_{oc} = 0.86–0.90 V), indicating the observed polymer regularity effects on solar cell performance are not due to the differences in polymer–polymer energy level alignments. However, the regularity of the polymer backbone greatly affect the J_{sc} and FF of the resulting APSCs. The decrease of EQEs (Figure S6, Supporting Information) with increasing *x* in either the donor or acceptor polymer further confirmed the effect of main chain regularity and polymer crystallinity on APSC performance. Moreover, substantial EQEs (Figure S5, Supporting Information) in the wavelength range from 650 to 850 nm were observable for all PTAZ-TPD*x*:PNDI-T*x* blends, indicating efficient hole transfer from the excited polymer acceptor to the polymer donor. As a consequence, the photon energy loss E_{loss}, which is defined by E_g–eV_{oc}, of all PTAZ-TPD*x*:PNDI-T*x* solar cells is relative low (≈0.6 eV), demonstrating the potential of APSCs for further performance improvement.

2.4. Charge Generation and Transport in the Blends

The exciton dissociation in blend films was investigated by steady-state photoluminescence (PL) quenching experiments. The PL spectra of the PTAZ-TPD*x*:PNDI-T*x* blends and the relevant neat polymers are presented in Figure S7 (Supporting Information). The PL quenching efficiency (ΔPL) was estimated by the PL intensity of the PTAZ-TPD*x*:PNDI-T*x* blends relative to that of the pure polymers (Table S8, Supporting Information). The PL of the donor (ΔPL_D) and the acceptor (ΔPL_A) in all donor:acceptor blends is almost completely quenched (ΔPL_D, ΔPL_A >95%). This suggests efficient exciton dissociation via charge transfer at the donor:acceptor interface in each PTAZ-TPD*x*:PNDI-T*x* blend, regardless of the regularity of the main chain of the donor or/and acceptor polymers.

Single photon counting time-resolved fluorescence experiments were further conducted to estimate the exciton lifetime of the neat polymers PTAZ-TPD*x* and PNDI-T*x*. The transient fluorescence traces of the polymers show essentially mono-exponential decay (Figure S8, Supporting Information). As shown in **Figure 3**a, the exciton lifetime of PTAZ-TPD00 is ≈880 ps, and decreases to ≈730 ps for PTAZ-TPD10 and further to ≈630 ps for PTAZ-TPD20. On the other hand, the PNDI-T*x* polymers show slightly longer exciton lifetimes when increasing the *x* value. The exact reason for this difference in change in PL lifetime with increasing *x* for the donor and acceptor polymers is not known at present, but it is likely related to the different extent by which trap sites are introduced by disorder and the reduced exciton diffusion by which such quenching sites are reached. A prolonged exciton lifetime is beneficial for the diffusion of the excitons to the donor:acceptor interface. Thus, the decrease of exciton lifetime upon increasing the content of TPD units in PTAZ-TPD*x* contributes to the observed decrease in EQEs and J_{sc}s of the resulting APSCs, but the decrease of device

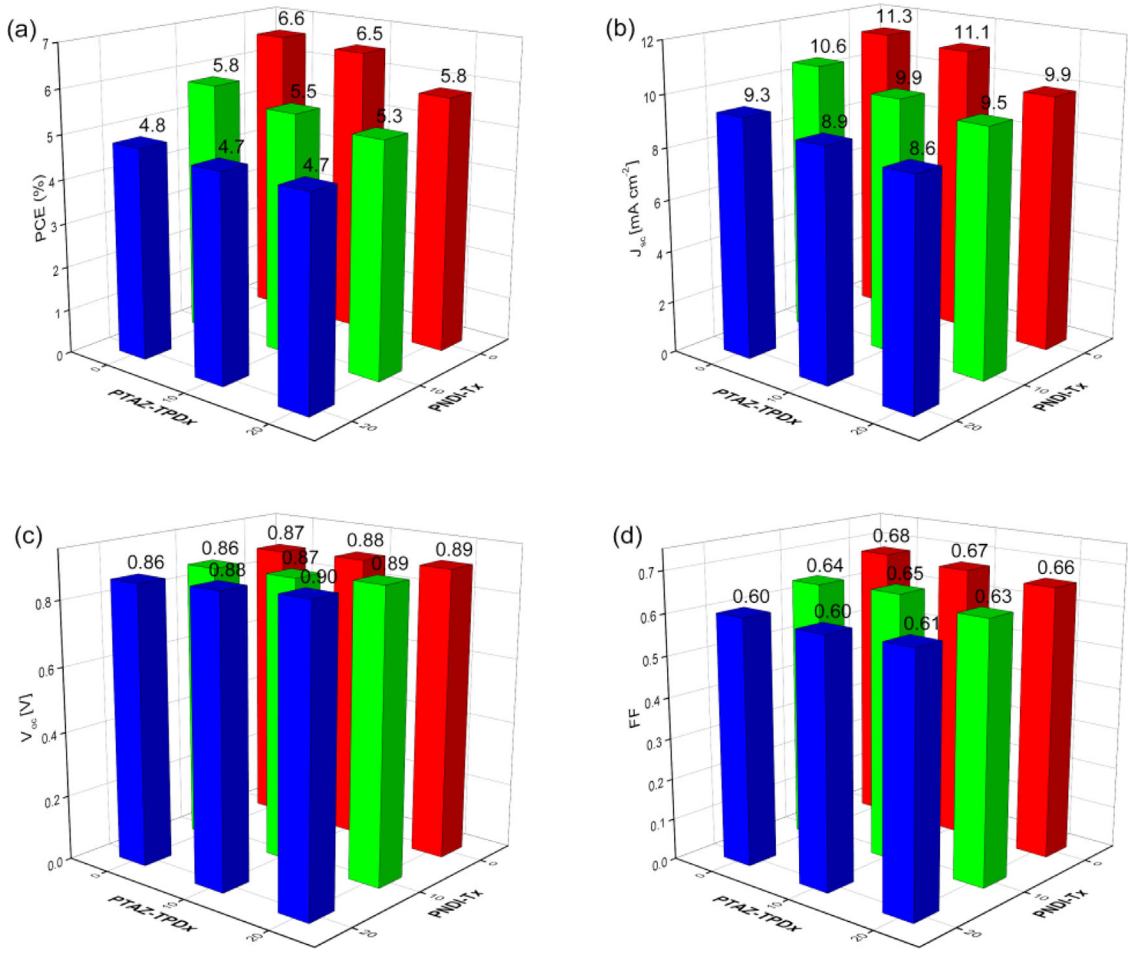

Figure 2. Photovoltaic parameters of the optimized PTAZ-TPD*x*:PNDI-T*x* solar cells acquired under AM1.5G illumination (100 mW cm^{-2}): a) PCE, b) J_{sc}, c) V_{oc}, and d) FF.

performance for the case of reducing the regularity of acceptor polymers PNDI-T*x* are dominated by other factors.

The hole and electron mobilities of PTAZ-TPD*x*:PNDI-T*x* blends were measured by the space-charge-limited current method using single charge carrier devices. The results are shown in Figure 3b, Figure S9 and Table S8 (Supporting Information). All PTAZ-TPD*x*:PNDI-T*x* blends show hole and electron mobilities on the order of 10^{-4} cm^2 V^{-1} s^{-1}, which is typical for APSCs.[10c] Except for PTAZ-TPD20:PNDI-T10 and PTAZ-TPD20:PNDI-T20, the hole mobilities of other blends are comparable ($\approx 3 \times 10^{-4}$ cm^2 V^{-1} s^{-1}), suggesting the hole transport is not largely affected by the *x* value in PTAZ-TPD*x*. The exception is PTAZ-TPD20, for which the hole mobility in the blend decreases when the regularity of the acceptor polymer is

Table 2. Photovoltaic parameters of the optimized PTAZ-TPDx:PNDI-Tx solar cells acquired under AM1.5G illumination (100 mW cm^{-2}).

Donor	Acceptor	V_{oc} [V]	J_{sc} [mA cm^{-2}]	FF	PCE [%]	EQE$_{max}$ [%]	E_{loss} [eV]
PTAZ-TPD00	PNDI-T00	0.87	11.3	0.68	6.6	59	0.59
	PNDI-T10	0.86	10.6	0.64	5.8	58	0.62
	PNDI-T20	0.86	9.3	0.60	4.8	53	0.63
PTAZ-TPD10	PNDI-T00	0.88	11.1	0.67	6.5	57	0.58
	PNDI-T10	0.87	9.9	0.65	5.5	53	0.61
	PNDI-T20	0.88	8.9	0.60	4.7	50	0.61
PTAZ-TPD20	PNDI-T00	0.89	9.9	0.66	5.8	52	0.57
	PNDI-T10	0.89	9.5	0.63	5.3	51	0.59
	PNDI-T20	0.90	8.6	0.61	4.7	49	0.59

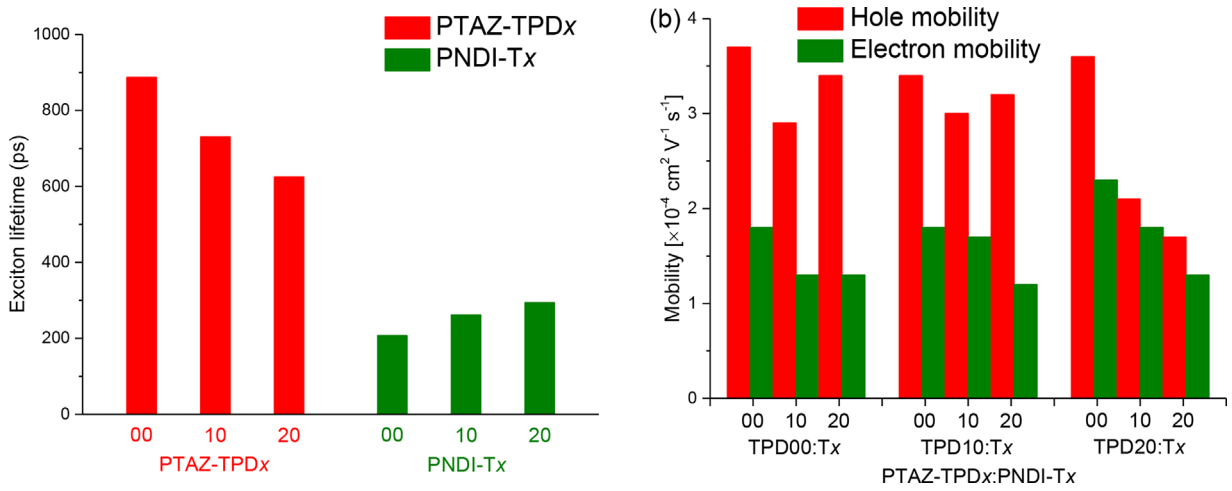

Figure 3. a) Exciton lifetime of PTAZ-TPD*x* and PNDI-T*x*; b) Hole mobility and electron mobility acquired from SCLC single-carrier devices of the PTAZ-TPD*x*:PNDI-T*x* blend films. The standard deviation for the charge carrier mobility is $\approx 0.3 \times 10^{-4}\,cm^2\,V^{-1}\,s^{-1}$.

increased (Figure 3b). This suggests that increasing x in the acceptor polymer reduces the crystallinity of the donor polymers in the blends (see section 2.5). The electron mobilities of the blends, however, decrease slightly along with reducing the regularity of the main chain of the acceptor polymers PNDI-T*x* regardless of the donor polymer used. In agreement with the DSC results discussed above (Figure S3, Supporting Information), reducing the degree of backbone regularity of PNDI-T*x* is expected to hinder π–π stacking, thus hampering intermolecular charge transport and reducing the electron mobility in the blends. The results indicate that the electron is the slower charge carrier in each PTAZ-TPD*x*:PNDI-T*x* blend. Under this circumstance, the charge transport related device parameters like EQE, J_{sc}, and FF are more susceptible to fluctuations of the electron mobility.[14] This observation is consistent with the decrease of EQE, J_{sc}, FF, and PCE along with the increase of x in the acceptor polymers PNDI-T*x* regardless of the donor polymer used. When comparing the PTAZ-TPD00:PNDI-T00 blend to the PTAZ-TPD20:PNDI-T20 blend we see that the PCE drops from 6.6 to 4.7% (a 29% relative decrease). In part this can now be rationalized by the concomitant losses in hole mobility ($3.7 \times 10^{-4} \rightarrow 1.7 \times 10^{-4}\,cm^2\,V^{-1}\,s^{-1}$, a 54% loss), electron mobility ($1.8 \times 10^{-4} \rightarrow 1.3 \times 10^{-4}\,cm^2\,V^{-1}\,s^{-1}$, a 28% loss), and the reduced donor excited state lifetime (830 → 630 ps, a 29% loss). We note, however, that the reduction of these parameters and hence the drop in PCE is likely originating from reducing crystallinity and domain size (see section 2.5). Overall, the above data demonstrate that the charge transport properties of the all-polymer blends can be optimized via the regularity of the polymer main chains and using the proper combination of these polymers.

The bimolecular charge recombination in the PTAZ-TPD*x*:PNDI-T*x* blends was studied by measuring the J_{sc} as a function of the light intensity (P_{light}). The relevant characteristics are shown in Figure S10 (Supporting Information). In all PTAZ-TPD*x*:PNDI-T*x* combinations, the power law exponent α (in $J_{sc} \propto P_{light}^{\alpha}$) is almost unity, suggesting bimolecular recombination is small at short circuit. The almost balanced hole and electron mobilities in the blends (differing by less than a factor 2 for PTAZ-TPD00:PNDI-T00) are consistent with the relatively high FFs (0.60–0.68) of the APSCs.

2.5. Film Morphology

The molecular packing structure and bulk crystallinity of the donor polymers PTAZ-TPD*x* and the acceptor polymers PNDI-T*x* as neat films were investigated by grazing incidence wide-angle X-ray scattering (GIWAXS).[15] The two-dimensional scattering patterns and line-cut profiles are shown in **Figure 4**. The lattice parameters are summarized in **Table 3**. In pure films, all PTAZ-TPD*x* and PNDI-T*x* films adopt a face-on orientation, with the (010) diffraction corresponding to the π–π stacking appearing in the out-of-plane direction and the lamellar peak in the in-plane direction. Such a face-on orientation is favorable to the efficient charge transport in vertical direction in solar cell devices. For both the neat donor polymers PTAZ-TPD*x* and the acceptor polymers PNDI-T*x*, increasing backbone disorder not only affects the π–π stacking in the out-of-plane direction, but also the lamellar packing in the in-plane direction, as seen from the change of diffraction peaks and crystal coherence length (CCL). The peak at $q \approx 1.55\,Å^{-1}$ is composed out of two signals belonging to the polymer donor (010) peak and the scattering signal of substrate. Both the π–π distance and lamellar (100) distance of PTAZ-TPD*x* increase with increasing the content of TPD units. When fitting peaks with Gaussian functions, we can clearly see that the (010) CCL of PTAZ-TPD*x* decreases with the addition of TPD units. Particularly, PTAZ-TPD20 shows almost the substrate scattering peak and weak film peak. The (100) CCL of the donor polymers also decreases from 7.23 nm for PTAZ-TPD00 to 6.15 nm for PTAZ-TPD20. These results confirmed the decrease of polymer crystallinity and packing order of the PTAZ-TPD*x* polymers by reducing the regularity of the backbone,[10a,16] even though clear melting and crystallization transitions were not observed in DSC. As expected, the π–π distance of PNDI-T*x* increases with increasing the content of single thiophene units due to the increased backbone twist and

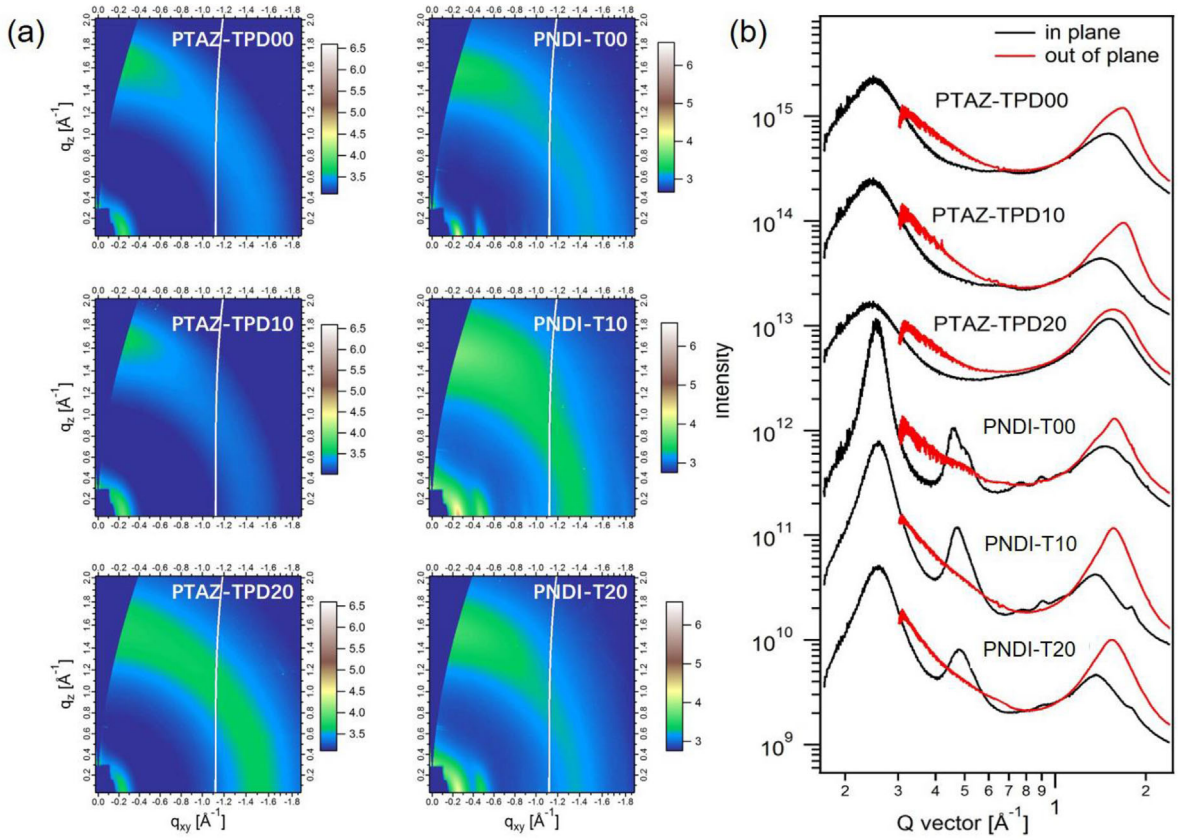

Figure 4. GIWAXS of the neat films of PTAZ-TPD*x* and PNDI-T*x*: a) 2D diffraction patterns, and b) line-cut profiles.

disorder.[10a,10c] It has been demonstrated that the FF of polymer solar cells decrease along with enlarging the polymer π–π stacking distance,[17] which is consistent with the FF differences in our devices. More interestingly, the CCLs of both π–π stacking and lamellar stacking decrease along with increasing the *x* value of PNDI-T*x*. Specifically, the (100) CCL of PNDI-T00 is 18.87 nm, indicating a highly crystalline film, while the (100) CCL of PNDI-T10 and PNDI-T20 are 13.02 and 10.01 nm, respectively. The (200) peak also weakens when increasing the thiophene units. These results suggest a progressively decreasing polymer crystallinity for PNDI-T*x* by adding more single thiophene units. Overall, modulation of the crystallinity of both donor polymers PTAZ-TPD*x* and acceptor polymers PNDI-T*x* has been achieved by random copolymerization.

Table 3. Lattice parameters of the polymers PTAZ-TPD*x* and PNDI-T*x* in neat films.

	π–Stacking (010)		Lamellar (100)	
Polymer	d_{010} [nm]	CCL [nm]	d_{100} [nm]	CCL [nm]
PTAZ-TPD00	0.367	2.50	2.50	7.23
PTAZ-TPD10	0.366	2.20	2.55	7.03
PTAZ-TPD20	0.400	0.74	2.60	6.15
PNDI-T00	0.397	2.13	2.47	18.87
PNDI-T10	0.402	2.08	2.44	13.02
PNDI-T20	0.406	1.71	2.44	10.01

The morphology of the PTAZ-TPD*x*:PNDI-T*x* blends was first characterized by bright-field transmission electron microscopy (TEM). The results are shown in Figure S11 and S12 (Supporting Information). Unfortunately, the results are not informative enough to resolve the morphology differences of the PTAZ-TPD*x*:PNDI-T*x* blends due to the weak contrast between the two polymers. Therefore, the blends of PTAZ-TPD00:PNDI-T*x* and PTAZ-TPD*x*:PNDI-T00 were further studied by GIWAXS. Notably, GIWAXS can closely characterize morphology properties such as local crystallinity and domain size.[9b,10a] The two-dimensional scattering patterns and line-cut profiles of blends are shown in **Figure 5** and the lattice parameters are summarized in **Table 4**. In the PTAZ-TPD00:PNDI-Tx blends the (100) peaks (Figure 5) can be attributed to the acceptor polymers because the shape is similar to that of acceptor films, while peaks of donor films are much wider (Figure 4). For these blends, the (010) peaks are dominated by the donor, but the acceptor also contributes to the crystallinity according to the shoulder peak at $q \approx 1.58$ Å^{-1}. A trifling decrease of (010) CCL can be calculated by fitting the curves when increasing the *x* value of PNDI-T*x*. The (100) CCL of the PTAZ-TPD00:PNDI-T*x* blends displays an obvious drop from 16.84 to 13.18 nm. The (200) peaks show the same trend as the pure acceptors and are reduced with adding single thiophene units. The attenuation of (100) and

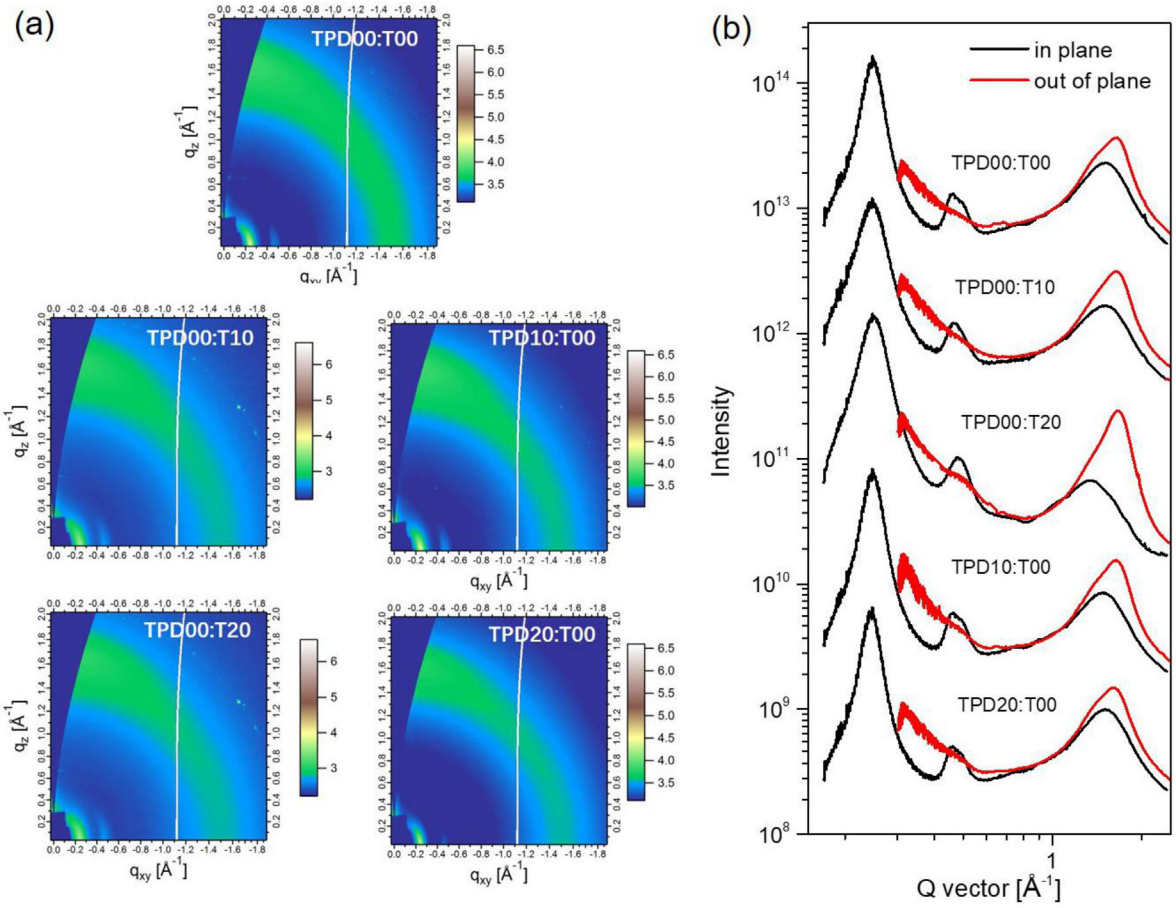

Figure 5. GIWAXS of the PTAZ-TPD*x*:PNDI-T*x* blend films: a) 2D diffraction patterns, and b) line-cut profiles.

(200) CCL indicates a worse local crystallinity and contracted domain size which explains the reduction of device performance. For PTAZ-TPD*x*:PNDI-T00 blends, the crystallinity is mainly dominated by PNDI-T00 acceptors instead of the PTAZ-TPD*x* donors. This is judged from the fact that (100) CCL of various PTAZ-TPD*x*:PNDI-T00 blends is close to the value for the pure PNDI-T00 film. We think that the fact that the CCL changes slightly and is smaller than in pure PDNI-T00, involves crystallinity and miscibility induced interactions. The slightly increased (100) CCL observed for the PTAZ-TPD20:PNDI-T00 compared to the other two PTAZ-TPD*x*:PNDI-T00 blends may be related to the lesser crystallinity of the donor. These small differences may account for the modest drop of device performance when changing the donors in blends for certain acceptor. All in all, the introduction of TPD units in PTAZ-TPD*x* has a mild influence on donor crystallization and domain size, while the introduction of single thiophene units in PNDI-T*x* exerts significant effects on acceptor crystallization and domain size, particularly on the lamellar stacking.

Table 4. Characteristic length scale of phase separation in blend films of PTAZ-TPDx:PNDI-Tx.

	π–π Stacking (010)		Lamellar (100)	
Blend	d_{010} [nm]	CCL [nm]	d_{100} [nm]	CCL [nm]
PTAZ-TPD00:PNDI-T00	0.376	2.85	2.524	16.84
PTAZ-TPD00:PNDI-T10	0.382	2.45	2.540	13.25
PTAZ-TPD00:PNDI-T20	0.390	2.37	2.516	13.18
PTAZ-TPD10:PNDI-T00	0.378	2.58	2.531	16.51
PTAZ-TPD20:PNDI-T00	0.381	2.46	2.556	17.46

2.6. Coarse-Grained Modeling of Polymer–Polymer Blend Morphology

Understanding polymer–polymer blend film morphology with a simplified physical model provides a different and complementary perspective.[9b,11,18] Molecular dynamics simulations with a coarse-grained model were carried out to get a better understanding of the morphological features of the polymer–polymer blend films. The details for the modelling are presented in the Supporting Information. The simulated morphological features of the blends with varying the *x* value of either polymer donor and polymer acceptor in PTAZ-TPD*x*:PNDI-T*x* blend are shown in Figure S13, Supporting Information. The modeling results provide useful information in terms of domain size and crystallinity. The domain size *R*

Table 5. Domain sizes and bond direction correlations of the PTAZ-TPDx:PNDI-Tx blends.

		Bond direction correlation	
Blend	Domain size [nm]	PTAZ-TPDx	PNDI-Tx
PTAZ-TPD00:PNDI-T00	16.4	0.686	0.833
PTAZ-TPD00:PNDI-T10	13.2	0.660	0.763
PTAZ-TPD00:PNDI-T20	12.3	0.665	0.738
PTAZ-TPD10:PNDI-T00	15.7	0.675	0.811
PTAZ-TPD20:PNDI-T00	15.3	0.660	0.807

can be obtained from the integration of the first moment of the structure factor,

$$R = 2\pi \frac{\sum_{q=0}^{q=q_c} S_{(q)}}{\sum_{q=0}^{q=q_c} qS(q)}, \quad (1)$$

where q_c is a cutoff wave vector, which is taken as 0.46 nm^{-1}. As listed in **Table 5**, the average domain size of the PTAZ-TPD00:PNDI-Tx blends displays an obvious drop from 16.4 to 12.3 nm from PNDI-T00 to PNDI-T20. For PTAZ-TPDx:PNDI-T00 blends, a mild drop from 16.4 to 15.8 nm was observed when increasing the x value of PTAZ-TPDx. These results are consistet with the (100) CCL obtained from GIWAXS data.

The bond direction correlation (BDC) of interacted polymer units which describes the local order parameter could be used to evaluate crystallinity,

$$\mathrm{BDC} = \sum_{N} \left|\vec{r}_{ij} \cdot \vec{r}_{kl}\right| / N, \qquad r_{ik,\, il,\, jk \text{ or } jl} < r_{\mathrm{cut}} \quad (2)$$

where $\vec{r}$ is the unit vector of polymer bond between two adjacent monomer units with the indexes of i and j or k and l, N the contact number, and the cutoff radius of interaction $r_{\mathrm{cut}} = 4.8$ nm. The value of BDC is in the range of 0–1.0, where 0 indicates complete chaos and 1.0 indicates perfect crystal. The BDC of both PTAZ-TPDx and PNDI-Tx in blends are given in Table 5. As x increases, the overall crystallinity of PTAZ-TPD00:PNDI-Tx blends obviously decreases, while the overall crystallinity of PTAZ-TPDx:PNDI-T00 slightly decreases. The dominant crystalline polymer in the blends is PNDI-Tx. Therefore, the introduction of single thiophene units exerts a more significant effect than TPD units on crystallinity and domain size, which is consistent with experimental results.

3. Conclusion

In conclusion, we synthesized a set of TAZ-based donor polymers PTAZ-TPDx and NDI-based acceptor polymers PNDI-Tx via random copolymerization with the intention to fine-tune the polymer crystallinity and nanostructure of the resulting donor:acceptor blends. By increasing the x value in PTAZ-TPDx and PNDI-Tx, we were able to reduce the polymer crystallinity monotonically. We find a negligible effect of the regularity of the polymer main chain on the optical absorption properties and energy levels. The characterization of all-polymer solar cells, however, reveals that reducing the crystallinity of either donor polymer or acceptor polymer leads to a steady decrease of the EQEs, J_{sc}, FF, and consequently the PCEs of the devices. The decrease of polymer crystallinity contributes to a lowering of the domain size of phase separation in donor:acceptor blends as disclosed by GIWAXS measurements and coarse-grained molecular dynamic simulations. Moreover, upon increasing the polymer disorder we observed reduced exciton lifetimes of the pure donors PTAZ-TPDx and reduced electron mobilities for the acceptor polymers PNDI-Tx, which ultimately affects charge generation and charge transport in the resulting blends. These observations explain the acquired device metrics including EQEs, J_{sc}, FF, and PCEs. We note that in previous comparisons of PNDI-T00 (N2200) and PNDI-T10 with other donor polymers, PNDI-T10 was found to give higher efficiencies than PNDI-T00.[6f,10c] In these studies, the number-average molecular weights of PNDI-T10 was more than double of that of PNDI-T00. Hence it seems that for these acceptor polymers a higher molecular weight can compensate for the lower crystallinity in achieving higher performance. The different observations can also be related to the miscibility between the polymer donor and polymer acceptor.[10d] Since different polymer donors were used in these studies, the different miscibility may lead to different crystallinity requirement to realize proper phase separation. Thus, a rational molecular design strategy for high-performance APSCs should consider the miscibility between polymer donor and polymer acceptor at the same time. Overall, this work demonstrates an important strategy to modulate the miscibility and morphology of the blends, thus to optimize APSC performance, through tuning the crystallinity of both donor and acceptor polymers.

Supporting Information

Supporting Information is available from the Wiley Online Library or from the author.

Acknowledgments

The work was performed in the framework of the Mujulima (EU-FP7, No. 604148) and Triple Solar (ERC Adv Grant No. 339031) projects, and received funding from the Ministry of Education, Culture and Science of Netherlands (Gravity program 024.001.035). This work was also supported by the Recruitment Program of Global Youth Experts of China and the Ministry of Science and Technology (2017YFA0206600). Thanks for the support from Ministry of science and technology (2016YFA0200700), NSFC (21504066, 21534003). E.W. further acknowledges the Swedish Research Council and Formas for financial support. X-ray data were acquired at beamlines 7.3.3 and 11.0.1.2 at the Advanced Light Source, which is supported by the Director, Office of Science, Office of Basic Energy Sciences, of the U.S. Department of Energy under Contract No. DE-AC02-05CH11231.

Keywords

all-polymer solar cells, crystallinity, device performance, morphology

Received: September 5, 2018
Published online: September 27, 2018

[1] a)A. J. Heeger, *Adv. Mater.* **2014**, *26*, 10. b)Y. Li, G. Xu, C. Cui, Y. Li, *Adv. Energy Mater.* **2017**, *7*, 1701791.

[2] a)X. Che, Y. Li, Y. Qu, S. R. Forrest, *Nat. Energy* **2018**, *3*, 422. b) Z. Xiao, X. Jia, L. Ding, *Sci. Bull.* **2017**, *62*, 1562. c)Y. Zhang, B. Kan, Y. Sun, Y. Wang, R. Xia, X. Ke, Y. Q. Q. Yi, C. Li, H. L. Yip, X. Wan, Y. Cao, Y. Chen, *Adv. Mater.* **2018**, *30*, 1707508. d)S. Li, L. Ye, W. Zhao, H. Yan, B. Yang, D. Liu, W. Li, H. Ade, J. Hou, *J. Am. Chem. Soc.* **2018**, *140*, 7159.

[3] a)J. C. Hummelen, B. W. Knight, F. LePeq, F. Wudl, J. Yao, C. L. Wilkins, *J. Org. Chem.* **1995**, *60*, 532. b)M. M. Wienk, J. M. Kroon, W. J. H. Verhees, J. Knol, J. C. Hummelen, P. A. van Hal, R. A. J. Janssen, *Angew. Chem. Int. Ed.* **2003**, *42*, 3371.

[4] a)C. Yan, S. Barlow, Z. Wang, H. Yan, A. K. Y. Jen, S. R. Marder, X. Zhan, *Nat. Rev. Mater.* **2018**, *3*, 18003. b)P. Cheng, G. Li, X. Zhan, Y. Yang, *Nat. Photonics* **2018**, *12*, 131. c)J. Hou, O. Inganäs, R. H. Friend, F. Gao, *Nat. Mater.* **2018**, *17*, 119. d)C. B. Nielsen, S. Holliday, H.-Y. Chen, S. J. Cryer, I. McCulloch, *Acc. Chem. Res.* **2015**, *48*, 2803. e)H. Kang, W. Lee, J. Oh, T. Kim, C. Lee, B. J. Kim, *Acc. Chem. Res.* **2016**, *49*, 2424. f)C. Duan, G. Zango, M. García Iglesias, F. J. M. Colberts, M. M. Wienk, M. V. Martínez-Díaz, R. A. J. Janssen, T. Torres, *Angew. Chem. Int. Ed.* **2017**, *56*, 148. g)C. Duan, D. Guzmán, F. J. M. Colberts, R. A. J. Janssen, T. Torres, *Chem. Eur. J.* **2018**, *24*, 6339. h)X. Liu, B. Xie, C. Duan, Z. Wang, B. Fan, K. Zhang, B. Lin, F. J. M. Colberts, W. Ma, R. A. J. Janssen, F. Huang, Y. Cao, *J. Mater. Chem. A* **2018**, *6*, 395.

[5] a)W. Li, W. S. C. Roelofs, M. Turbiez, M. M. Wienk, R. A. J. Janssen, *Adv. Mater.* **2014**, *26*, 3304. b)J. W. Jung, J. W. Jo, C.-C. Chueh, F. Liu, W. H. Jo, T. P. Russell, A. K. Y. Jen, *Adv. Mater.* **2015**, *27*, 3310. c) J. Jung, W. Lee, C. Lee, H. Ahn, B. J. Kim, *Adv. Energy Mater.* **2016**, *6*, 1600504. d)C. Dou, X. Long, Z. Ding, Z. Xie, J. Liu, L. Wang, *Angew. Chem. Int. Ed.* **2016**, *55*, 1436. e)Y. Wang, Z. Yan, H. Guo, M. A. Uddin, S. Ling, X. Zhou, H. Su, J. Dai, H. Y. Woo, X. Guo, *Angew. Chem. Int. Ed.* **2017**, *56*, 15304. f)H.-H. Cho, S. Kim, T. Kim, V. G. Sree, S.-H. Jin, F. S. Kim, B. J. Kim, *Adv. Energy Mater.* **2017**, *7*, 1701436. g)S. Liu, X. Song, S. Thomas, Z. Kan, F. Cruciani, F. Laquai, J.-L. Bredas, P. M. Beaujuge, *Adv. Energy Mater.* **2017**, *7*, 1602574. h) X. Liu, C. Zhang, C. Duan, M. Li, Z. Hu, J. Wang, F. Liu, N. Li, C. J. Brabec, R. A. J. Janssen, G. C. Bazan, F. Huang, Y. Cao, *J. Am. Chem. Soc.* **2018**, *140*, 8934.

[6] a)S. Liu, Z. Kan, S. Thomas, F. Cruciani, J.-L. Brédas, P. M. Beaujuge, *Angew. Chem. Int. Ed.* **2016**, *55*, 12996. b)Z.-G. Zhang, Y. Yang, J. Yao, L. Xue, S. Chen, X. Li, W. Morrison, C. Yang, Y. Li, *Angew. Chem. Int. Ed.* **2017**, *56*, 13503. c)S. Liu, Y. Firdaus, S. Thomas, Z. Kan, F. Cruciani, S. Lopatin, J.-L. Bredas, P. M. Beaujuge, *Angew. Chem. Int. Ed.* **2018**, *57*, 531. d)N. Zhou, H. Lin, S. J. Lou, X. Yu, P. Guo, E. F. Manley, S. Loser, P. Hartnett, H. Huang, M. R. Wasielewski, L. X. Chen, R. P. H. Chang, A. Facchetti, T. J. Marks, *Adv. Energy Mater.* **2014**, *4*, 1300785. e)X. Gu, Y. Zhou, K. Gu, T. Kurosawa, Y. Guo, Y. Li, H. Lin, B. C. Schroeder, H. Yan, F. Molina-Lopez, C. J. Tassone, C. Wang, S. C. B. Mannsfeld, H. Yan, D. Zhao, M. F. Toney, Z. Bao, *Adv. Energy Mater.* **2017**, *7*, 1602742. f) Z. Li, W. Zhang, X. Xu, Z. Genene, D. Di Carlo Rasi, W. Mammo, A. Yartsev, M. R. Andersson, R. A. J. Janssen, E. Wang, *Adv. Energy Mater.* **2017**, *7*, 1602722. g)T. Kim, J.-H. Kim, T. E. Kang, C. Lee, H. Kang, M. Shin, C. Wang, B. Ma, U. Jeong, T.-S. Kim, B. J. Kim, *Nat. Commun.* **2015**, *6*, 8547. h)X. Long, Z. Ding, C. Dou, J. Zhang, J. Liu, L. Wang, *Adv. Mater.* **2016**, *28*, 6504.

[7] a)L. Gao, Z.-G. Zhang, L. Xue, J. Min, J. Zhang, Z. Wei, Y. Li, *Adv. Mater.* **2016**, *28*, 1884. b)X. Xu, Z. Li, W. Zhang, X. Meng, X. Zou, D. Di Carlo, Rasi, W. Ma, A. Yartsev, M. R. Andersson, R. A. J. Janssen, E. Wang, *Adv. Energy Mater.* **2017**, *7*, 1700908. c)B. Fan, L. Ying, P. Zhu, F. Pan, F. Liu, J. Chen, F. Huang, Y. Cao, *Adv. Mater.* **2017**, *29*, 1703906. d)Z. Li, X. Xu, W. Zhang, X. Meng, Z. Genene, W. Ma, W. Mammo, A. Yartsev, M. R. Andersson, R. A. J. Janssen, E. Wang, *Energy Environ. Sci.* **2017**, *10*, 2212. e)B. Fan, L. Ying, Z. Wang, B. He, X.-F. Jiang, F. Huang, Y. Cao, *Energy Environ. Sci.* **2017**, *10*, 1243. f)Y. Guo, Y. Li, O. Awartani, H. Han, J. Zhao, H. Ade, H. Yan, D. Zhao, *Adv. Mater.* **2017**, *29*, 1700309. g)D. Chen, J. Yao, L. Chen, J. Yin, R. Lv, B. Huang, S. Liu, Z. G. Zhang, C. Yang, Y. Chen, Y. Li, *Angew. Chem. Int. Ed.* **2018**, *57*, 4580. h)B. Fan, P. Zhu, J. Xin, N. Li, L. Ying, W. Zhong, Z. Li, W. Ma, F. Huang, Y. Cao, *Adv. Energy Mater.* **2018**, *9*, 1703085.

[8] H. Yan, Z. Chen, Y. Zheng, C. Newman, J. R. Quinn, F. Dötz, M. Kastler, A. Facchetti, *Nature* **2009**, *457*, 679.

[9] a)C. R. McNeill, *Energy Environ. Sci.* **2012**, *5*, 5653. b)N. Zhou, A. S. Dudnik, T. I. N. G. Li, E. F. Manley, T. J. Aldrich, P. Guo, H.-C. Liao, Z. Chen, L. X. Chen, R. P. H. Chang, A. Facchetti, M. Olvera de la Cruz, T. J. Marks, *J. Am. Chem. Soc.* **2016**, *138*, 1240.

[10] a)Y.-J. Hwang, T. Earmme, B. A. E. Courtright, F. N. Eberle, S. A. Jenekhe, *J. Am. Chem. Soc.* **2015**, *137*, 4424. b)S. Sharma, N. B. Kolhe, V. Gupta, V. Bharti, A. Sharma, R. Datt, S. Chand, S. K. Asha, *Macromolecules* **2016**, *49*, 8113. c)Z. Li, X. Xu, W. Zhang, X. Meng, W. Ma, A. Yartsev, O. Inganäs, M. R. Andersson, R. A. J. Janssen, E. Wang, *J. Am. Chem. Soc.* **2016**, *138*, 10935. d) T. Kurosawa, X. Gu, K. L. Gu, Y. Zhou, H. Yan, C. Wang, G.-J. N. Wang, M. F. Toney, Z. Bao, *Adv. Energy Mater.* **2017**, *7*, 1701552.

[11] G. Wang, N. D. Eastham, T. J. Aldrich, B. Ma, E. F. Manley, Z. Chen, L. X. Chen, M. O. de la Cruz, R. P. H. Chang, F. S. Melkonyan, A. Facchetti, T. J. Marks, *Adv. Energy Mater.* **2018**, *8*, 1702173.

[12] a)H. Kang, M. A. Uddin, C. Lee, K.-H. Kim, T. L. Nguyen, W. Lee, Y. Li, C. Wang, H. Y. Woo, B. J. Kim, *J. Am. Chem. Soc.* **2015**, *137*, 2359. b) S. Chen, Y. An, G. K. Dutta, Y. Kim, Z.-G. Zhang, Y. Li, C. Yang, *Adv. Funct. Mater.* **2017**, *27*, 1603564. c)K. D. Deshmukh, R. Matsidik, S. K. K. Prasad, L. A. Connal, A. C. Y. Liu, E. Gann, L. Thomsen, J. M. Hodgkiss, M. Sommer, C. R. McNeill, *Adv. Funct. Mater.* **2018**, *28*, 1707185.

[13] D. Veldman, S. C. J. Meskers, R. A. J. Janssen, *Adv. Funct. Mater.* **2009**, *19*, 1939.

[14] a)P. W. M. Blom, V. D. Mihailetchi, L. J. A. Koster, D. E. Markov, *Adv. Mater.* **2007**, *19*, 1551. b)J. A. Bartelt, D. Lam, T. M. Burke, S. M. Sweetnam, M. D. McGehee, *Adv. Energy Mater.* **2015**, *5*, 1500577.

[15] a)H. Alexander, B. Wim, G. James, S. Eric, G. Eliot, K. Rick, M. Alastair, C. Matthew, R. Bruce, P. Howard, *J. Phys. Conf. Ser.* **2010**, *247*, 012007. b)Y. Wu, Z. Wang, X. Meng, W. Ma, *Prog. Chem.* **2017**, *29*, 93.

[16] a)C. Duan, K. Gao, J. J. van Franeker, F. Liu, M. M. Wienk, R. A. J. Janssen, *J. Am. Chem. Soc.* **2016**, *138*, 10782. b)C. Duan, K. Gao, F. J. M. Colberts, F. Liu, S. C. J. Meskers, M. M. Wienk, R. A. J. Janssen, *Adv. Energy Mater.* **2017**, *7*, 1700519.

[17] J. M. Szarko, J. Guo, Y. Liang, B. Lee, B. S. Rolczynski, J. Strzalka, T. Xu, S. Loser, T. J. Marks, L. Yu, L. X. Chen, *Adv. Mater.* **2010**, *22*, 5468.

[18] a)C.-K. Lee, C.-W. Pao, C.-W. Chu, *Energy Environ. Sci.* **2011**, *4*, 4124. b)R. Alessandri, J. J. Uusitalo, A. H. de Vries, R. W. A. Havenith, S. J. Marrink, *J. Am. Chem. Soc.* **2017**, *139*, 3697.

